Dithieno[2,3-d:2′,3′-d′]benzo[1,2-b:4,5-b′]dithiophene (DTBDAT)-Based Copolymers for High-Performance Organic Solar Cells

Ye Seul Lee,[1] Seyeong Song,[2] Yung Jin Yoon,[2] Yun-Ji Lee,[3] Soon-Ki Kwon,[3] Jin Young Kim,[2] Yun-Hi Kim[1]

[1]Department of Chemistry & RINS, Gyeongsang National University, Jin-ju 660-701, Republic of Korea
[2]Department of Energy Engineering, Ulsan National Institute of Science and Technology (UNIST) Ulsan 689-798, South Korea
[3]Department of Materials Engineering and Convergence Technology, Gyeongsang National University, Jin-ju 660-701, Republic of Korea
Correspondence to: Y.-H. Kim (E-mail: ykim@gnu.ac.kr) or J. Y. Kim (E-mail: jykim@unist.ac.kr) or S.-K. Kwon (E-mail: skwon@gnu.ac.kr)

Received 17 May 2016; accepted 8 June 2016; published online 2 July 2016
DOI: 10.1002/pola.28205

ABSTRACT: **P(BDT-TCNT)** and **P(DTBDAT-TCNT)**, which has an extended conjugation length, were designed and synthesized for applications in organic solar cell (OSCs). The solution absorption maxima of **P(DTBDAT-TCNT)** with the extended conjugation were red-shifted by 5–15 nm compared with those of **P(BDT-TCNT)**. The optical band gaps and highest occupied molecular orbital (HOMO) energy levels of both **P(BDT-TCNT)** and **P(DTBDAT-TCNT)** were similar. The structure properties of thin films of these materials were characterized using grazing-incidence wide-angle X-ray scattering and tapping-mode atomic force microscopy, and charge carrier mobilities were characterized using the space-charge limited current method. OSCs were formed using [6,6]-phenyl-C_{71}-butyric acid methyl ester ($PC_{71}BM$) as the electron acceptor and 3% diphenylether as additive suppress aggregation. OSCs with **P(BDT-TCNT)** as the electron donor exhibited a power conversion efficiency (PCE) of 4.10% with a short-circuit current density of $J_{SC} = 9.06$ mA/cm^2, an open-circuit voltage of $V_{OC} = 0.77$ V, and a fill factor of $FF = 0.58$. OSCs formed using **P(DTBDAT-TCNT)** as the electron donor layer exhibited a PCE of 5.83% with $J_{SC} = 12.2$ mA/cm^2, $V_{OC} = 0.77$ V, and $FF = 0.62$. © 2016 Wiley Periodicals, Inc. J. Polym. Sci., Part A: Polym. Chem. **2016**, *54*, 3182–3192

KEYWORDS: conjugated polymers; synthesis; structure-property relations

INTRODUCTION Polymer solar cells (PSCs) have received growing attention in recent years owing to the flexible, colorful and low-mass properties of the devices, and the broad range of potential small- and large-area applications.[1,2] PSCs typically employ bulk-heterojunction (BHJ) architecture, and the power conversion efficiencies (PCEs) of PSCs that have thus far been achieved range from 1% to more than 9%.[3–6] One strategy that has been employed to achieve a PCE is the use of donor–acceptor (D-A) conjugated polymers with alternating electron-rich (donor) and electron-deficient (acceptor) moieties. The electronic properties of these layers can be easily tuned by controlling the intermolecular charge transfer from the donor to the acceptor.[7–10] The most important parameter of PCE is the open-circuit voltage V_{oc}, which is related to the optical band gap E_g.[11]

The copolymer unit 2,3-bis-(thiophene-2-yl)-acrylronitrile has a vinyl linkage with a nitrile group between thiophene units. This group can increase the conjugation length, which lead to a decrease in the band gap. Moreover, the nitrile group can attract electrons through the vinyl linkage. Therefore, 2,3-bis-(thiophene-2-yl)-acrylronitrile can be used as an acceptor. The copolymer unit (4,8-bis(4,5-didecylthiophen-2-yl)benzo[1,2-*b*:4,5-*b*′]dithiophene-2,6-iyl)bis(trimethylstannane) (BDT) is known to be electron-rich unit with a high charge carrier mobility and high V_{oc} and BDT has been widely used as the donor unit for high-performance organic photovoltaics.[12–16] Fused derivatives of BDT such as dithieno[2,3-*d*:2′,3′-*d*′]benzo[1,2-*b*:4,5-*b*′]dithiophene (DTBDAT) for use as donor units in polymers provide a higher PCE than BDT when combined with a 2,3-bis-(thiophene-2-yl)-acrylronitrile acceptor unit.[17,18] Such fused aromatic rings typically exhibit excellent intermolecular charge-transport properties because of the planarity of the backbone. There have been several reports describing the high charge-carrier mobilities of these moieties when used in organic field-effect transistors.[2,19] Derivatives of DTBDAT exhibit relatively low HOMO levels and large band gaps compared with those of other fused aromatic rings, which suggests that the DTBDAT

Y. S. Lee and S. Song contributed equally to this work.

© 2016 Wiley Periodicals, Inc.

motif is a particularly stable organic semiconductor. Although the development of materials based on DTBDAT is expected to lead to promising printable organic semiconductors, materials formed from DTBDAT moieties have not been reported.[20] DTBDAT can be prepared using a TCNT moiety as an electron acceptor unit, which helps to strengthen the intermolecular interactions between polymer chains, resulting in relatively large charge carrier mobility. Here we investigate the structural properties of **P(BDT-TCNT)** and **P(DTBDAT-TCNT)** with extended conjugations for applications in organic thin film transistor (TFTs) and organic solar cells (OSCs).[23]

EXPERIMENTAL

Characterization

^{1}H-NMR and ^{13}C NMR spectra were recorded with a Bruker Advance-300 and 500 spectrometer. The thermal analysis were performed on a TA TGA 2100 thermogravimetric analyzer in a nitrogen atmosphere at a rate of 10 °C/min. Differential scanning calorimeter (DSC) was conducted under nitrogen on a TA instrument 2100 DSC. The sample was heated with 10 °C/min from 30 to 300 °C. UV–vis absorption spectra were measured by UV-1650PC spectrophotometer. Molecular weights and polydispersities of the copolymers were determined by gel permeation chromatography (GPC) analysis with polystyrene standard calibration (waters high-pressure GPC assembly Model M515 pump, μ-Styragel columns of HR4, HR4E, HR5E, with 500 and 100 Å, refractive index detectors, solvent: tetrahydrofuran). Cyclic voltammetry (CV) was performed on an EG and G Parc model 273 Å potentiostat/galvanostat system with a three-electrode cell in a solution of 0.1 M tetrabutylammonium perchlorate (Bu_4NClO_4) in acetonitrile at a scan rate of 50 mV/s. The polymer films were coated on a square carbon electrode by dipping the electrode into the corresponding solvents and then dried under nitrogen. A Pt wire was used as the counter electrode, and an $Ag/AgNO_3$ (0.1 M) electrode was used as the reference electrode. Atomic force microscopy (AFM) images of the polymer:$PC_{71}BM$ blend films were recorded on a XE-100 (Park systems) with an AC160-TS cantilever in the tapping mode. AFM samples were fabricated in the same method for OPV devices without TiO2/Al deposition. Photoluminescence (PL) spectra of the polymer:$PC_{71}BM$ blends were obtained on a Horiba Jobin Yvon spectrometer (iHR320, FL 3-1 iHR, S1 detector). Transmission electron microscopy (TEM) images were taken on Philips CM30 microscope at an operating voltage of 300 keV. For TEM experiments, the polymer:$PC_{71}BM$ blend films spin-coated on the ITO/PEDOT:PSS substrates were floated in water, and then lifted on a carbon-coated square mesh copper grid (#200 mesh). The electronic structures and conformations of model compounds of polymer backbone in study were estimated by density functional theory (DFT) calculations. The model compound consisted of three repeating units of polymers were geometrically optimized to an energy minimum using Gaussian 09 at the DFT B3LYP level with a 6-31 + G(d,p) basis set. To save the calculation time, all the alkyl chains were shortened to methyl groups.

Materials

The $Pd_2(dba)_3$ and $P(o\text{-}tol)_3$ were purchased from Umicore. All reactions were carried out in a nitrogen atmosphere using the usual Schlenk techniques. All chemical reagents were purchased from Aldrich and used as received. Other chemicals were used unless otherwise specified.

Synthesis of (E)−2,3-Bis(5-bromothiophene-2-yl)acrylonitrile (1)

Compound 1 was synthesized referring to the literature.[21]

^{1}H NMR (300 MHz, $CDCl_3$, δ): 7.27 (d, 1 H), 7.22 (s, 1 H), 7.10–7.08 (m, 2 H), 7.03 (d, 1 H). ^{13}C NMR (75 MHz, $CDCl_3$, δ): 140.3, 139.2, 139.0, 132.7, 131.9, 127.9, 127.5, 120.1, 118.8, 117.1, 109.3. FTIR (cm^{-1}): 3025, 2214, 1584, 1429, 1409, 1313, 905, 787, 500.

Synthesis of (E)−2,3-Bis(5-(trimethylstannyl) thiophene-2-yl)acrylonitrile (2)

Compound 2 was synthesized referring to the literature.[22]

^{1}H NMR (300 MHz, $CDCl_3$, δ): 7.66–7.65 (d, 1 H), 7.56 (s, 1 H), 7.43–7.42 (d, 1 H), 7.22–7.21 (d, 1 H), 7.15–7.13 (d, 1 H), 0.53–0.32 (m, 18 H). ^{13}C NMR (75 MHz, $CDCl_3$, δ) 144.38, 143.30, 139.77, 136.12, 135.67, 132.82, 131.57, 127.79, 117.50, 102.37, −8.10, −8.16. FTIR (cm^{-1}): 3058 (aromatic, C-H), 2996–2800 (aliphatic, C-H), 2218 (-CN), 1576–1408 (C = C).

Synthesis of 4,8-Bis(4,5-didecylthiophen-2-yl)benzo [1,2-b:4,5-b′]dithiophene (3)

Compound 3 was synthesized referring to the literature.[23]

^{1}H NMR (300 MHz, $CDCl_3$, δ): 7.69 (d, 2 H), 7.46 (d, 2 H), 7.23 (s, 2 H), 2.85 (br, 4 H), 2.62 (t, 4 H), 1.72 (m, 8 H), 1.72 (m, 8 H), 1.30 (m, 56 H), 0.90 (t, 12 H).

Synthesis of (4,8-Bis(4,5-didecylthiophen-2-yl)benzo [1,2-b:4,5-b′]dithiophene-2,6-diyl)bis(trimethylstannane) (4)

Compound 4 was also synthesized referring to the literature.[23]

^{1}H NMR (300 MHz, $CDCl_3$, δ): 7.74 (s, 2 H), 7.24 (s, 2 H), 2.85 (t, 4 H), 2.63 (t, 4 H), 1.70 (m, 8 H), 1.29 (m, 56 H), 0.90 (t, 12 H), 0.41 (t, 18 H). FTIR (cm^{-1}): 3108 (aromatic, C-H), 2923–2855 (aliphatic, C-H).

Synthesis of 5-10-Bis(4,5-didecylthiophen-2-yl)benzo [1,2-b:4,5-b′]diithieno[3,2-b]thiophene (5)

Compound 5 was synthesized referring to the literature.[19]

^{1}H NMR (300 MHz, $CDCl_3$, δ): 7.47–7.45 (d, $J = 5.12$ Hz, 2 H), 7.31–7.29 (d, $J = 6.02$, 2 H), 7.12 (s, 2 H), 2.93–2.70 (m, 8 H), 2.17–2.15 (m, 8 H), 1.60–1.41 (m, 56 H), 0.92–0.89 (m, 12 H); ^{13}C NMR (75 MHz, $CDCl_3$, δ): 143.8, 143.4, 142.3, 139.7, 139.6, 134.4, 132.8, 131.4, 130.7, 130.2, 124.7, 120.5, 32.77, 32.71, 31.61, 30.49, 30.43, 30.37, 30.23, 30.15, 30.06, 29.07, 28.78, 23.47, 14.63; EIMS (m/z (%)): 1027 [M^+]

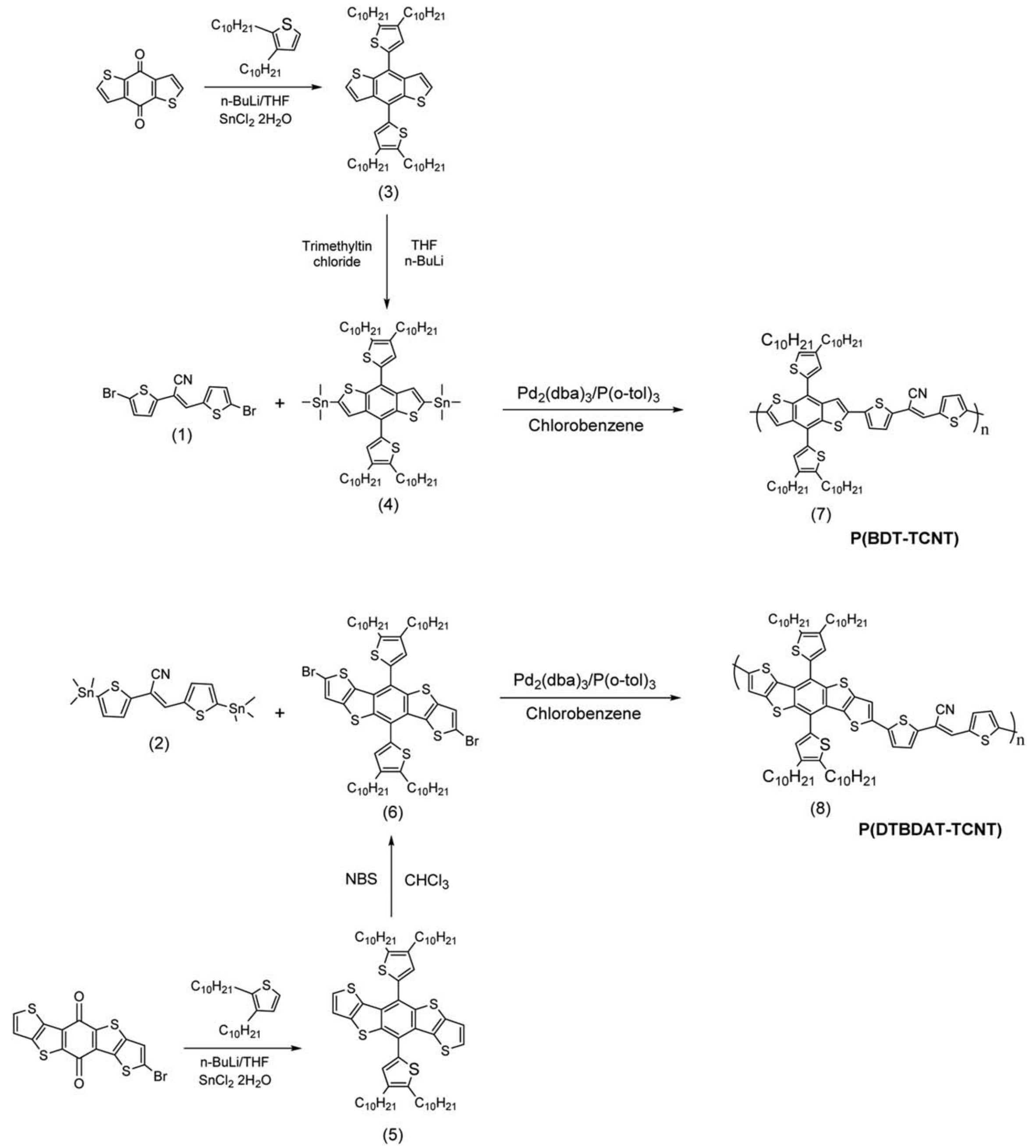

SCHEME 1 Synthetic scheme of polymers (P(BDT-TCNT) and P(DTBDAT-TCNT)).

Synthesis of 2,7-Dibromo-5,10-bis(4,5-didecylthiophen-2-yl)benzo[1,2-b:4,5-b′]diithieno[3,2-b]thiophene (6)

Under nitrogen atmosphere, compound 5 (4.0 g, 3.43 mmol) was dissolved into chloroform. N-bromosuccinimide (NBS) (1.5 g, 8.59 mmol) was added to the solution slowly. The reaction mixture was stirred at room temperature for 12 h. The reaction mixture was poured into water and extracted with dichloromethane. The organic solution was dried with plenty of anhydrous magnesium sulfate and evaporation with low pressure. The compound was further purified by recrystallization from dichloromethane and isopropyl alcohol (Yield: 4.1g, 72%). ^{1}H NMR (300 MHz, $CDCl_3$, δ): 7.31 (s, 2 H), 7.09 (s, 2 H), 2.95–2.90 (t, 4 H), 2.72–2.67 (t, 4 H), 1.82–1.70 (m, 8 H), 1.51–1.31 (m, 56 H), 0.92–0.87 (m, 12 H). FTIR (cm^{-1}): 3092 (aromatic, C-H), 2916–2848 (aliphatic, C-H).

Polymerization of P(BDT-TCNT)

In a 25 mL dry flask, compound 4 (0.4000 g, 0.322 mmol) and compound 1 (0.1208 g, 0.322 mmol) was dissolved in 6 mL chlorobenzene, then bubbling with nitrogen for 30 min. Pd_2 $(dba)_3$ (5.9 mg, 0.006 mmol) and $P(o\text{-}tol)_3$ (7.8 mg, 0.025 mmol) were added to the mixture, which was stirred for 48 h at 110 °C afterwards. Tributyl(thiophen-2-

(a) P(BDT-TCNT)

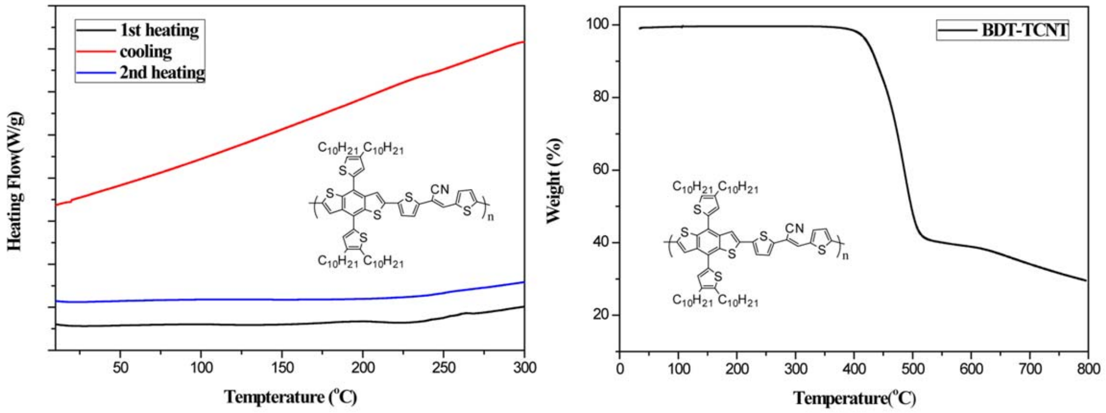

(b) P(DTBDAT-TCNT)

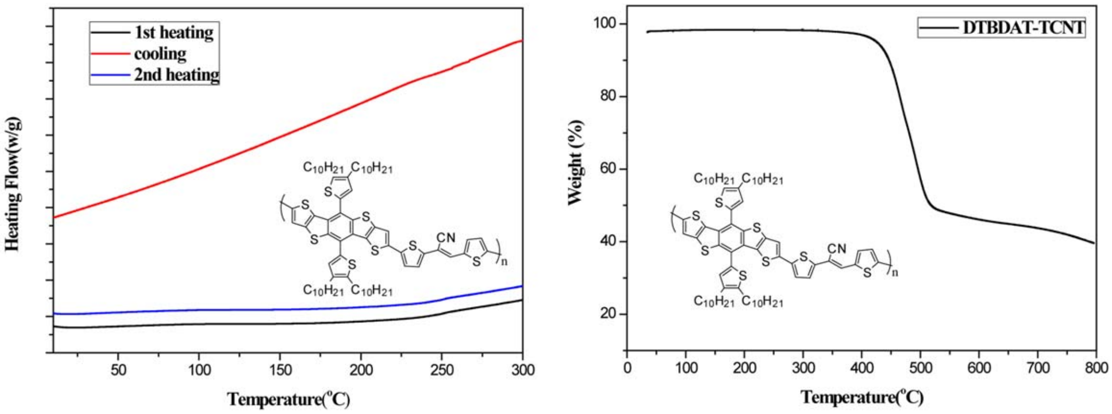

FIGURE 1 TGA thermogram and DSC curve of (a) P(BDT-TCNT) and (b) P(DTBDAT-TCNT) at a heating rate of 10 °C/min. [Color figure can be viewed in the online issue, which is available at wileyonlinelibrary.com.]

yl)stannane and 2-bromothiophene were injected sequentially into the reaction mixture for end-capping, and the solution was stirred for 6 h after each addition. After cooling to room temperature, the reaction mixture was then dropped into methanol (100 mL). The crude polymer was collected by filtration and purified by soxhlet extraction with methanol, acetone, hexane and chloroform in sequence. The **P(BDT-TCNT)** was obtained by precipitation of the chloroform solution into methanol (Yield: 0.26 g)

^{1}H NMR (500 MHz, $CDCl_3$, δ): 7.80–7.46 (br, 3 H), 7.25–6.52 (br, 5 H), 2.94–2.74 (br, 8 H), 1.79–1.35 (br, 64 H), 0.91 (br, 12 H). FTIR (cm^{-1}): 3073 (aromatic, C-H), 2917–2854 (aliphatic, C-H), 2215 (-CN), 1658–1459 (C = C).

Polymerization of P(DTBDAT-TCNT)

In a 25-mL dry flask, compound 2 (0.4000 g, 0.337 mmol) and compound 6 (0.1831 g, 0.337 mmol) was dissolved in 6-mL chlorobenzene, then bubbling with nitrogen for 30 min. Pd_2 $(dba)_3$ (5.9 mg, 0.006 mmol) and $P(o\text{-}tol)_3$ (7.8 mg, 0.025 mmol) were added to the mixture, which was stirred for 48 h at 110 °C afterwards. Tributyl(thiophen-2-yl)stannane and 2-bromothiophene were injected sequentially into the reaction mixture for end-capping, and the solution was stirred for 6 h after each addition. After cooling to room temperature, the reaction mixture was then dropped into methanol (100 mL). The crude polymer was collected by filtration and purified by soxhlet extraction with methanol, acetone, hexane, and chloroform in sequence. The **P(DTBDAT-TCNT)** was obtained by precipitation of the chloroform solution into methanol (Yield: 0.13 g).

FTIR (cm^{-1}): 3071 (aromatic, C-H), 2930–2857 (aliphatic, C-H), 2215 (-CN), 1650–1453 (C = C).

RESULTS AND DISCUSSION

Scheme 1 shows the synthesis of **P(BDT-TCNT)** and **P(DTBDAT-TCNT)**. The monomers were synthesized according to the methods in references.[2,19,20,22] Polymers were obtained via a Stille coupling reaction using Pd_2 $(dba)_3$/$P(o\text{-}tol)_3$ (1/4) in chlorobenzene. **P(BDT-TCNT)** and **P(DTBDAT-TCNT)** were purified via Soxhlet extraction in methanol, hexane, and chloroform. The chloroform fraction was collected and reprecipitated in methanol. The chemical structures of **P(BDT-TCNT)** and **P(DTBDAT-TCNT)** were analyzed using proton nuclear magnetic resonance (H NMR) spectroscopy.

(a) P(BDT-TCNT)

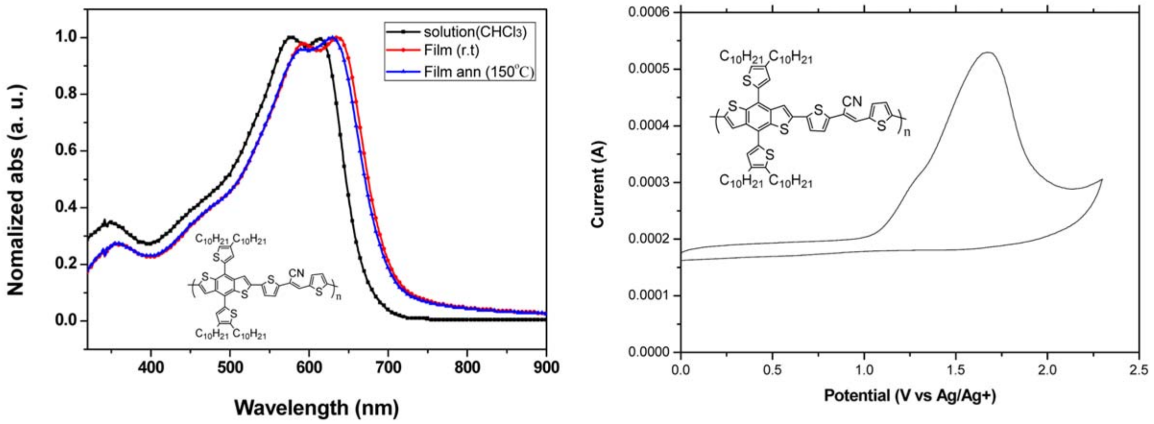

(b) P(DTBDAT-TCNT)

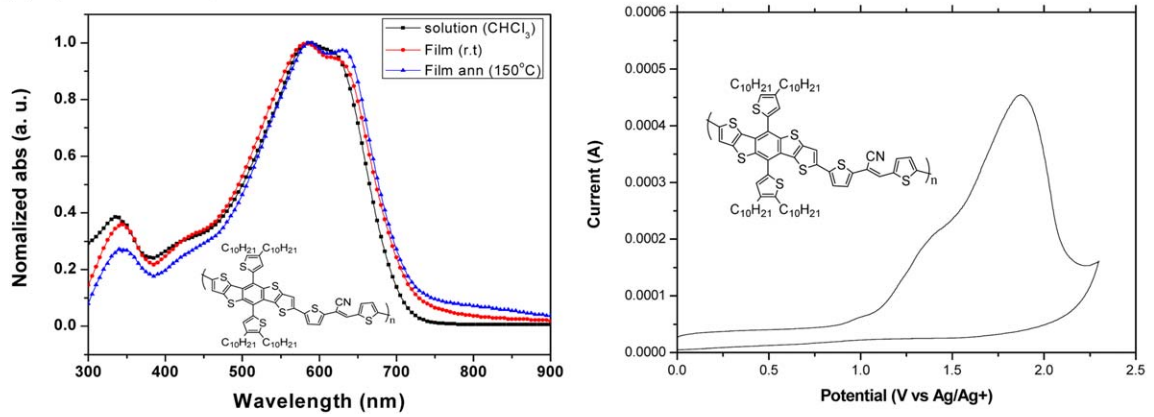

FIGURE 2 UV–vis absorption spectra and Cyclovoltammograms of (a) P(BDT-TCNT) and (b) P(DTBDAT-TCNT). [Color figure can be viewed in the online issue, which is available at wileyonlinelibrary.com.]

Both polymers were soluble in chloroform, chlorobenzene, and dichlorobenzene.

The thermal stability of the polymers was investigated using thermogravimetry analysis (TGA) with a heating rate of 10 °C/min in a nitrogen atmosphere. As shown in Figure 1, both **P(BDT-TCNT)** and **P(DTBDAT-TCNT)** exhibited good thermal stability, with 5% weight loss at 423 and 437 °C, respectively. Differencial scanning calorimetry (DSC) was used to investigate the phase behavior, and neither polymer exhibited any transitions between 50 and 300 °C.

UV–vis absorption spectra were measured in solution phase and as thin films. Figure 2 shows UV–vis absorption spectra of the two copolymers. In chloroform, **P(BDT-TCNT)** exhibited absorption maxima at 571 and 615 nm, and **P(DTBDAT-TCNT)** exhibited absorption maxima at 587 and 620 nm. The solution absorption maxima of **P(DTBDAT-TCNT)**, with the extended conjugation, red-shifted by 5–15 nm compared with those of **P(BDT-TCNT)**. In the thin film state, **P(BDT-TCNT)** exhibited absorption maxima at 592 and 634 nm, that is, the absorbance bands were red shifted by $\sim$20 nm, compared with solution-phase absorption spectra. **P(DTBDAT-TCNT)** exhibited absorption maxima at 584 and 626 nm, that is, little spectral shift was observed relative to solution phase spectra. This suggests planarity and rigidity of the polymer backbone, even in solution. Table 1 lists a summary of the optical properties of the two copolymers. The optical band gap of **P(BDT-TCNT)** was 1.73 eV and that of **P(DTBDAT-TCNT)** was 1.71 eV. These results are based on the onset of the absorption spectra. The electrochemical properties of two polymers were investigated using cyclic voltammetry. The oxidation onset of **P(BDT-TCNT)** and **P(DTBDAT-TCNT)** was 1.09 and 1.07 V, respectively. We determined the HOMOs based on the onset of oxidation from the equation $E^{\text{HOMO}} = -(E^{\text{OX}} + \text{ferrocene}^{\text{OX}})$, where E^{OX} is the oxidation onset potential of both polymers and ferrocene$^{\text{OX}}$

TABLE 1 The Optical Properties of P(BDT-TCNT) and P(DTBDAT-TCNT)

	P(BDT-TCNT)	P(DTBDAT-TCNT)
UV-S (max) (nm)	615, 571, 348	620, 587, 336
UV-F (max) (nm)	634, 592, 353	626, 584, 344
UV-F-ann (max) (nm)	630	633
UV-edge (nm)	714	724
Band gap (optical) (ev)	1.73	1.71
HOMO (ev)	−5.49	−5.49
LUMO (ev)	−3.76	−3.78

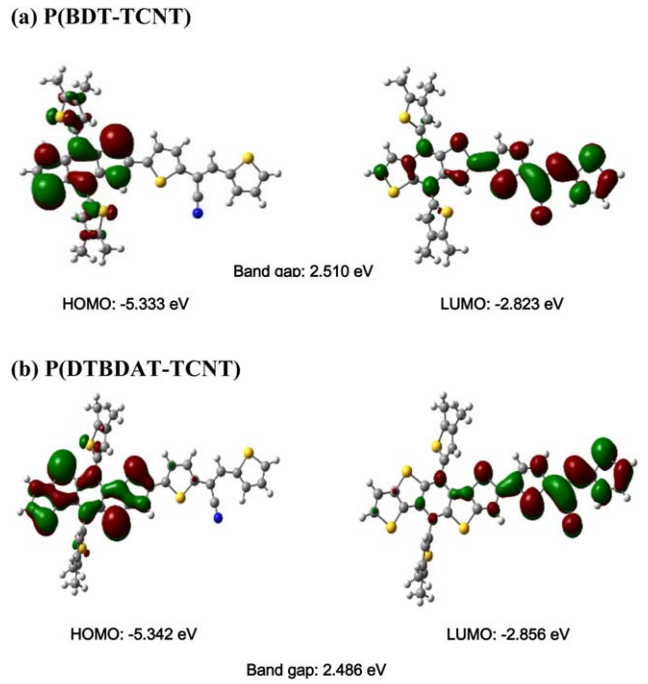

FIGURE 3 Calculated stereostructure and frontier orbital of P(BDT-TCNT) (upper) and P(DTBDAT-TCNT) (bottom). [Color figure can be viewed in the online issue, which is available at wileyonlinelibrary.com.]

is the oxidation onset potential of a ferrocene reference. The HOMO values are −5.49 eV for **P(BDT-TCNT)** and −5.47 eV for **P(DTBDAT-TCNT).** For both compounds, the LUMO levels were −3.76 eV, which were calculated from optical band gaps and HOMO levels of them. The difference between the LUMO levels of these polymers and $PC_{71}BM$ suggests that the energy offset will be sufficient to give rise to efficient charge transfer/separation at polymer/$PC_{71}BM$ interfaces. Moreover, the relatively low HOMO levels are expected to give rise to a large V_{oc}.

The electronic density distributions of the polymers were analyzed using density functional theory (DFT). Figure 3 shows the resulting molecular orbitals and energy levels.

TABLE 2 Photovoltaic Properties of the Polymers Blended with $PC_{71}BM$ at 1:1 Weight Chlorobenzene (CB) with or Without Diphenylether (DPE)

	P(BDT-TCNT)		P(DTBDAT-TCNT)	
CB:DPE (v/v)	100:0	97:3	100:0	97:3
J_{sc} (mA/cm^2)	2.65	9.06	5.69	12.20
V_{oc} (V)	0.77	0.78	0.75	0.77
FF	0.40	0.58	0.38	0.62
PCE (%)	0.82	4.10	1.62	5.83
Cal. J_{sc} (mA/cm^2)	2.64	8.71	5.55	11.93

The calculated energy levels are in good agreement with experimental data and both **P(DTBDAT- TCNT)** and **P(BDT-TCNT)** had similar HOMO and LUMO energy levels.

Fabrication and Characterization of Organic Solar Cells

Organic solar cells (OSCs) were fabricated with structure of indium tin-oxide-coated glass (ITO)/PEDOT:PSS/**P(BDT-TCNT)**:$PC_{71}BM$/Al. The patterned ITO was cleaned with detergent and rinsed by ultrasonic cleaner of distilled water, acetone, and isopropanol. Substrates were treated in an ultraviolet-ozone chamber for 20 min after dried in an oven at 100 °C. Poly(3,4-ethylenedioxythiophene):poly(styrene sulfonate) (PEDOT:PSS, Baytron P clevios^{TM} AI 4083, Germany) was spin-coated onto the ITO glass as 45 nm thin layer and dried at 140 °C for 10 min. Solutions containing mixture of **P(BDT-TCNT)**:$PC_{71}BM$ in chlorobenzene (CB) solvent with concentration of 1 wt % were spin-cast on the PEDOT:PSS layer under a nitrogen filled glove box. The mixed solutions of **P(BDT-TCNT)**:$PC_{71}BM$ include diphenylether (DPE) as an additive by 3% (v/v). Then, Al cathode (100 nm) was deposited on the active layer by thermal evaporation in vacuum ($<10^{-6}$ torr) condition. The thickness of the photoactive layer was measured using a surface profiler (KLA_tencor). The active area of the device was 13 mm^2. *J–V* characteristics were measured by a computer-controlled Keithley 2635A Source Measurement under an AM 1.5G illumination at 100

TABLE 3 The Parameters of OPV at Various Conditions

Polymer	Polymer:$PC_{71}BM$ (w/w)	Solvent (v/v)	J_{SC} (mA/cm^2)	V_{OC} (V)	*FF*	*PCE* (%)
P(BDT-TCNT)	1:1	CB	2.65	0.77	0.40	0.82
		97%CB: 3%DPE	9.06	0.78	0.58	4.10
		95%CB: 5%DPE	8.01	0.78	0.58	3.63
		90%CB: 10%DPE	7.85	0.75	0.59	3.49
		DCB	5.02	0.87	0.39	1.69
		97%DCB: 3%DPE	6.37	0.84	0.57	3.06
P(DTBDAT-TCNT)	1:1	CB	5.69	0.75	0.38	1.62
		97%CB: 3%DPE	12.2	0.77	0.62	5.83
		95%CB: 5%DPE	11.3	0.75	0.53	4.55
		DCB	11.3	0.77	0.59	4.76
		97%DCB: 3%DPE	11.1	0.77	0.55	4.69

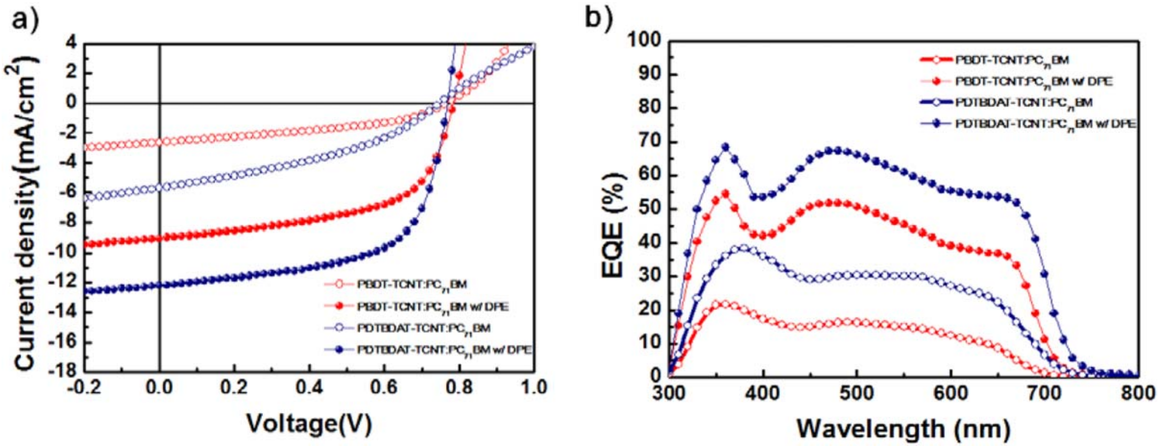

FIGURE 4 J–*V* characteristics and EQE spectra. [Color figure can be viewed in the online issue, which is available at wileyonlinelibrary.com.]

mW/cm^2. EQE (PV Measurements) spectra were obtained by applied monochromatic light from a xenon lamp.

Film Morphology and Solar Cell Performance

We investigated the effect of the benzodithiophene-based conjugate polymer including the cyano group as an electron unit and acceptor PC71BM matierials on the performance and film property of bulkheterojunction (BHJ) organic solar cells. Organic solar cells with configuration of conventional structure were fabricated with the ratio of 1:1 (w/w) blend of the conjugate polymer:PC$_{71}$BM in chlorobenzene (CB) as a photoactive material. To obtain optimal photoactive material, a small amount of additive a diphenylether (DPE) was used.[24],[25] Table 2 lists a summary of the device performance parameters and Table 3 lists parameters for each polymer device. The corresponding current density–voltage (*J*–*V*) characteristics and external quantum efficiency (EQE) spectra are shown in Figure 4. The best performance of device based on **P(DTBDAT-TCNT)**:PC$_{71}$BM (1:1 w/w) with 3% DPE exhibited a power conversion efficiency (PCE) of 5.83% with a current density $J_{SC} = 12.2$ mA/cm^2, open circuit voltage $V_{OC} = 0.77$ V, and a fill factor FF = 0.62.

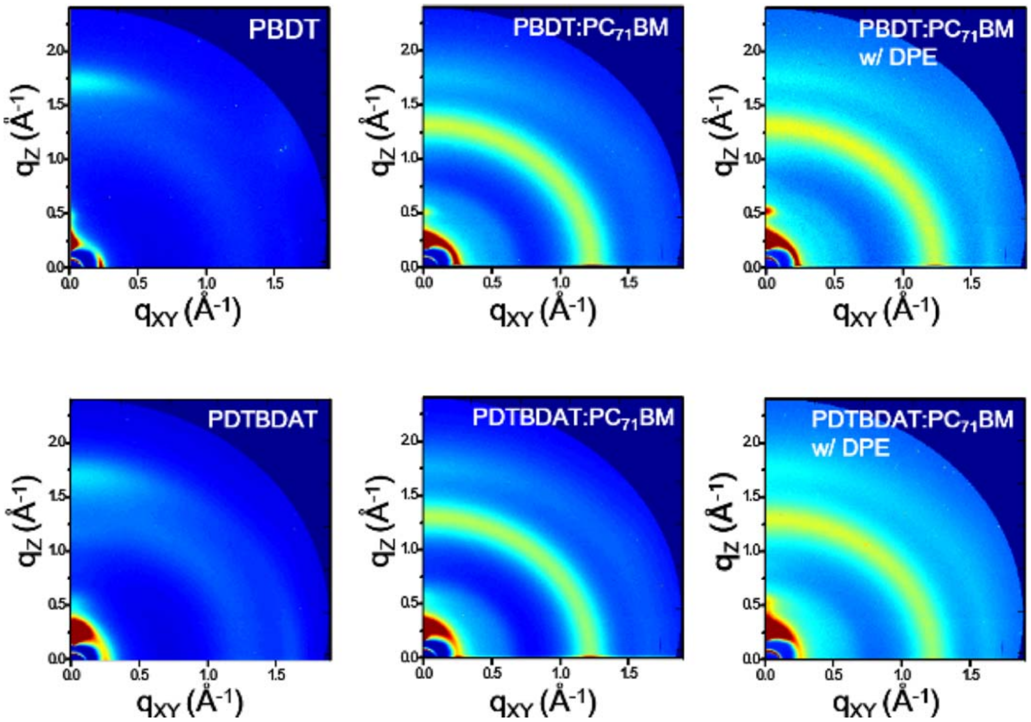

FIGURE 5 2D GIWAXS patterns of thin films as neat, Polymer:PC$_{71}$BM blend and blend with DPE as a processing additive for P(BDT-TCNT) (upper) and P(DTBDAT-TCNT) (bottom). [Color figure can be viewed in the online issue, which is available at wileyonlinelibrary.com.]

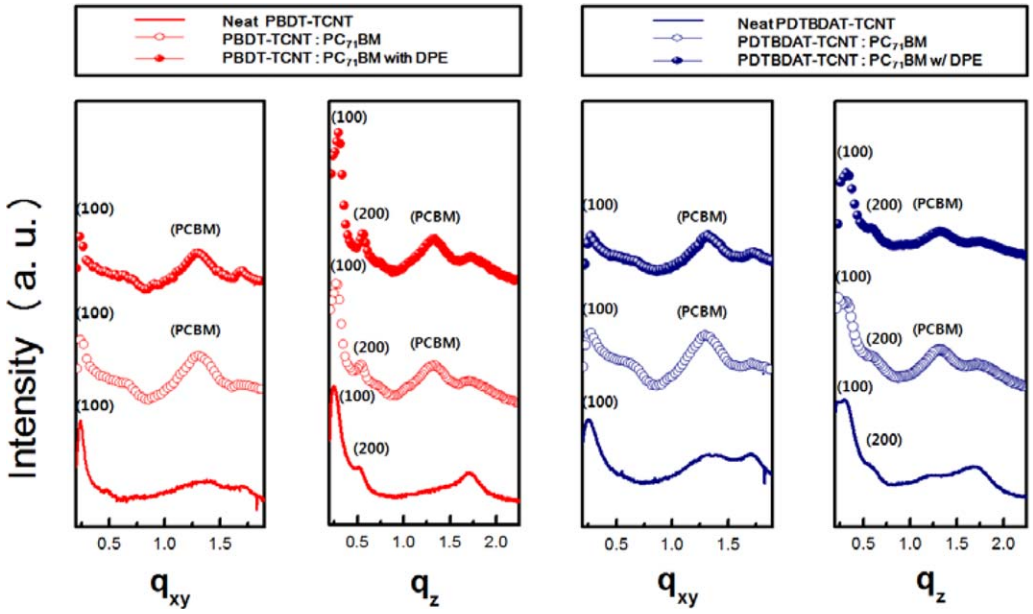

FIGURE 6 In-plane (q_{xy}) and out-of-plane (q_z) linecuts of polymer films: (a) The result of P(BDT-TCNT) (b) P(DTBDAT-TCNT). [Color figure can be viewed in the online issue, which is available at wileyonlinelibrary.com.]

The device formed using P(BDT-TCNT) exhibited $V_{OC} = 0.78$ V, which is similar to that of P(DTBDAT-TCNT); the PCE was 4.10%, with $J_{SC} = 9.06$ mA/cm^2 and $FF = 0.58$. Employing DPE as morphology processing additive in the CB solution significantly enhanced the short-circuit current density, which increased from $J_{SC} = 2.65$ and $J_{SC} = 5.69$ without DPE to $J_{SC} = 9.06$ and $J_{SC} = 12.2$ mA/cm^2 with DPE for OSCs based on P(BDT-TCNT):$PC_{71}BM$ and P(DTBDAT-TCNT):$PC_{71}BM$, respectively, and the corresponding PCEs increased to 4.10% and 5.83%. In the data shown in Figure 4, J_{SC} was calculated by integrating the EQE spectra. The data are consistent with the J_{SC} calculated from J–V curves (agreement to within ±3%), which indicates that these OSC measurements were reliable.

To investigate the relationship between the microstructural arrangement of the polymers in thin films and the performance of OSCs, we measured grazing-incidence wide-angle X-ray scattering (GIWAXS) and analyzed the film patterns of pristine polymers and optimal polymer:$PC_{71}BM$ blends. Both pristine and blended films exhibited (h00) diffraction patterns along q_z (out-of-plane) with q_{xy} (in-plane) corresponding to lamella ordering. Furthermore, (010) peaks were observed along all axes, which indicates π-π stacking of

TABLE 4 The Parameters of GIWAXS Data

	Direction	Scattering Vector (q) of π–π Stacking (Å^{-1})	d-Spacing (Å)	Lamella Interaction (h00)	Scattering Vector of Lamella Peak (Å^{-1})	Lamella Interaction Distance (Å)
Neat-P(BDT-TCNT)	In-plane (q_{xy})	1.72	3.65	(100)	0.23	27.32
	Out-of-plane (q_z)	1.72	3.65	(100)	0.25	25.13
P(BDT-TCNT):$PC_{71}BM$	In-plane (q_{xy})	1.73	3.63	(100)	0.24	26.18
	Out-of-plane (q_z)	1.75	3.59	(100)	0.28	22.44
P(BDT-TCNT):$PC_{71}BM$ w/DPE	In-plane (q_{xy})	1.72	3.65	(100)	0.23	27.32
	Out-of-plane (q_z)	1.75	3.59	(100)	0.27	23.27
Neat-P(DTBDAT-TCNT)	In-plane (q_{xy})	1.71	3.67	(100)	0.25	25.13
	Out-of-plane (q_z)	1.70	3.70	(100)	0.29	21.67
P(DTBDAT-TCNT):$PC_{71}BM$	In-plane (q_{xy})	1.72	3.65	(100)	0.26	24.17
	Out-of-plane (q_z)	1.77	3.55	(100)	0.32	19.63
P(DTBDAT-TCNT):$PC_{71}BM$ W/DPE	In-plane (q_{xy})	1.72	3.65	(100)	0.25	25.13
	Out-of-plane (q_z)	1.77	3.55	(100)	0.30	20.94

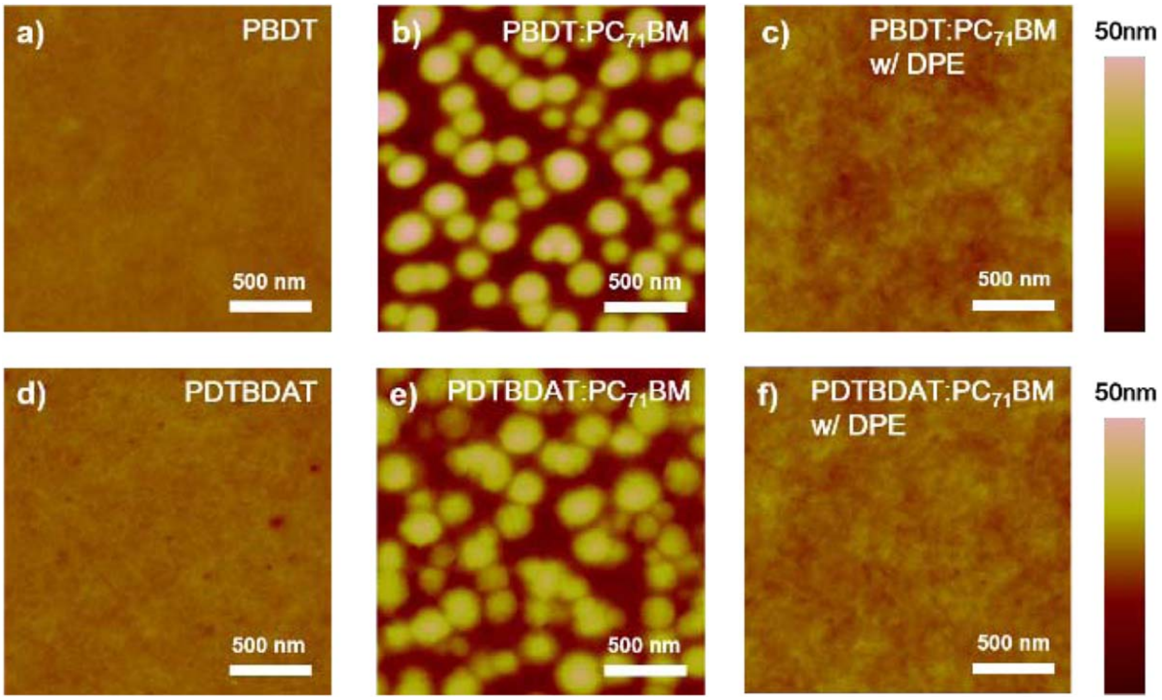

FIGURE 7 AFM morphology images (2 μm × 2 μm) of the pristine, Polymer:$PC_{71}BM$ blend and blend with 3% DPE (v/v) in Chlorobezene for P(BDT-TCNT) (a–c) and P(DTBDAT-TCNT (d–f). [Color figure can be viewed in the online issue, which is available at wileyonlinelibrary.com.]

the molecule backbones, as shown in Figures 5 and 6. Table 4 lists the crystallographic parameters.

Both of the pristine polymer films exhibited first- and second-order diffraction peaks up in the out-of-plane directions, indicating lamella stacking. The pristine **P(BDT-TCNT)** thin film exhibited strong inter-lamellar scattering peaks at 0.23–0.25 $Å^{-1}$ on both axis. In contrast, the pristine-**P(DTBDAT-TCNT)** film exhibited reflection at 0.25–0.29 $Å^{-1}$, indicating that the **P(DTBDAT- TCNT)**-based film had a shorter inter-lamella interaction distance (25.13–21.67 Å) than the films based on PBDT-TCNT (27.32–25.13 Å). These trends were also observed for the blended system, with the halo patterns at 1.31–1.35 $Å^{-1}$ which are attributed to the $PC_{71}BM$ acceptor. The scattering vector due to lamella stacking increased slightly from 0.23–0.25 to 0.23–0.28 $Å^{-1}$ of films based **P(BDT-TCNT)**, and increased from 0.25–0.29 Å to 0.26–0.32 $Å^{-1}$ for films based on **P(DTBDAT-TCNT)**. The π-π stacking peaks of the blended thin films along the q_z axis also changed following the addition of fullerene derivatives. For **P(BDT-TCNT)**, q_z increased from 1.72 $Å^{-1} \rightarrow 1.75$ $Å^{-1}$, and for **PDTBDAT-TCNT**, q_z increased from 1.70 $Å^{-1}$ $\rightarrow 1.77$ $Å^{-1}$) with narrower d-spacing by adding fullerene derivative materials compared to pristine films.

To investigate the surface morphology of thin films, we carried out tapping-mode atomic force microscopy (AFM) measurements, as shown in Figure 7. The topographic images of the neat-polymer indicate a root-mean-square (RMS) roughness of Rq = 3.35 nm for **P(BDT-TCN**T) and Rq = 1.87 nm of **P(DTBDAT-TCNT)**. Large agglomerated clusters were observed for the blended polymer:$PC_{71}BM$ film, which is consistent with inferior OSC performance; we found the RMS of 41.25 nm for **P(BDT-TCNT)**:$PC_{71}BM$, and 28.10 nm for **P(DTBDAT-TCNT)**:$PC_{71}BM$. Solution-phase DPE was added to control the morphology of the thin films, resulting in sufficient phase separation to enable efficient electron transport from the polymer to the $PC_{71}BM$ layer. The performances of PSCs formed devices with DPE processing were dramatically enhanced by over twice of J_{SC} value arising from evidently reduced RMS of 8.37 and 7.29 nm of **P(BDT-TCNT)**:$PC_{71}BM$

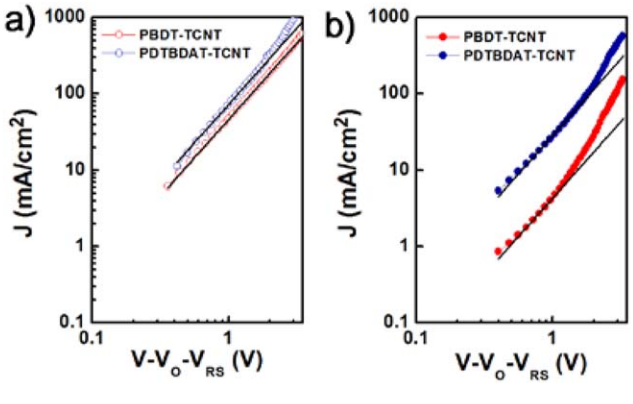

FIGURE 8 (a) Logarithmic plot of dark *J*–*V* characteristics from the hole-only devices and (b) electron-only device. [Color figure can be viewed in the online issue, which is available at wileyonlinelibrary.com.]

TABLE 5 Results of the SCLC Device Performance

Polymer	Thickness$_{electron}$ (nm)	$\mu_{electron}$ (cm^{2}V/s)	Thickness$_{hole}$ (nm)	μ_{hole} (cm^{2}V/s)	μ_e/μ_h
P(BDT-TCNT)	95	1.2 x 10^{-5}	140	4.2 x 10^{-4}	0.03
P(DTBDAT-TCNT)	90	6.9 x 10^{-5}	140	6.6 x 10^{-5}	1.04

and **P(DTBDAT-TCNT)**:PC$_{71}$BM films. The external photocurrent in bulkheterojunction (BHJ) solar cell systems corresponds to the photogenerated charge carriers that are extracted from the photoactive layer to the electrodes. Therefore, the charge carrier mobilities for holes and electrons are significant for device performance. We used the space-charge limited current (SCLC) method to investigate vertical transport of charge carrier. We fabricated hole only (ITO/PEDOT:PSS/polymer:PC$_{71}$BM/Au) and electron only (FTO/polymer:PC$_{71}$BM) devices using the optimized conditions described above. The SCLC carrier transport properties can be found using $J = 9\varepsilon_0\varepsilon_r\mu V^2/8L^3$, where ε_0 is permittivity of free-space, ε_r is the relative dielectric constant of the semiconductor, μ is the charge carrier mobility, V is the applied voltage and L is the thickness of the layer. Figure 8 shows the dark current versus the applied bias voltage, which was revised the built-in potential. Table 5 lists the electron and hole mobilities. We found $\mu_{hole} = 4.2\times10^{-4}$ cm^2/Vs and $\mu_{electron} = 1.2\times10^{-5}$ cm^2/Vs for **P(BDT-TCNT)**:PC$_{71}$BM, and $\mu_{hole} = 6.6\times10^{-5}$ cm^2/Vs and $\mu_{electron} = 6.9\times10^{-5}$ cm^2/Vs for **P(DTBDAT-TCNT)**:PC$_{71}$BM devices, respectively. The $\mu_{hole}/\mu_{electron}$ ratios greater than 1.04 were observed for devices formed of **P(DTBDAT-TCNT)**:PC$_{71}$BM and the ratio $\mu_{hole}/\mu_{electron}$ was 0.03 for **P(BDT-TCNT)**:PC$_{71}$BM, resulting in superior performance with a larger *FF* for the **P(DTBDAT-TCNT)**-based device.

CONCLUSIONS

We investigate the structure–property relations of newly designed and synthesized **P(BDT-TCNT)** and **P(DTBDAT-TCNT)** materials, the latter of which exhibits an extended conjugation length, for application in OSCs. The optical band gaps and HOMO energy levels were similar, OSCs formed with **P(BDT-TCNT)** exhibited a PCE of 4.10% with $J_{SC} = 9.06$ mA/cm^2, with $V_{OC} = 0.77$ V, and $FF = 0.58$. OSCs formed using **P(DTBDAT-TCNT)** exhibited a PCE of 5.83% with $J_{SC} = 12.2$ mA/cm^2, $V_{OC} = 0.77$ V, and $FF = 0.62$. The improved performance of the **P(DTBDAT-TCNT)**-based devices may be explained by considering the larger current due to shorter interlamella interaction, as a more balanced ratio $\mu_{hole}/\mu_{electron}$, resulting from extended conjugation of **P(DTBDAT-TCNT)**.

ACKNOWLEDGMENTS

This work was supported by the National Research Foundation (NRF) of Korea (2015R1A2A1A10055620 and 2015 M1A2A2057506) and MOTIE/KEIT(10048317).

REFERENCES AND NOTES

1 M. Wang, X. Hu, P. Liu, W. Li, X. Gong, F. Huang, Y. Cao, *J. Am. Chem. Soc.* **2011**, *133*, 9638–9641.

2 Kwon, J. Ho, An, J.–Y. Jang, H. Choi, S. Chung, D. S. Lee, M. Jung, Cha, H.–J. Park, J.–H. Park, C.–E. Kim, Y. –H. *J. Polym. Sci. Part A: Polym. Chem.* **2011**, *49*, 1119–1128.

3 H. Choi, J. P. Lee, S. J. Ko, J. W. Jung, H. Park, S. Yoo, O. Park, J. R. Jeong, S. Park, J. Y. Kim, *Nano Lett.* **2013**, *13*, 2204–2208.

4 T. L. Nguyen, H. Choi, S. J. Ko, M. A. Uddin, B. Walker, S. Yum, J. E. Jeong, M. H. Yun, T. J. Shin, S. Hwang, J. Y. Kim, H. Y. Woo, *Energ. Environ. Sci.* **2014**, *7*, 3040–3051.

5 H. Bin, Zhi-Guo Zhang, L. Gao, S. Chen, Lian Zhong, L. Xue, C. Yang, Y. Li, *J. Am. Chem. Soc.* **2016**, *138*, 4657–4664.

6 Jing-De Chen, C. Cui, Yan-Qing Li, L. Zhou, Qing-Dong Ou, C. Li, Y. Li, Jian-Xin Tang, *A. Material* **2015**, *27*, 1035–1041.

7 N. Wang, Z. Chen, W. Wei, Z. Jiang, *J. Am. Chem. Soc.* **2013**, *135*, 17060–17068.

8 E. Wang, Z. Ma, Z. Zhang, K. Vandewal, P. Henriksson, O. Inganäs, F. Zhang, M. R. Andersson, *J. Am. Chem. Soc.* **2011**, *133*, 14244–14247.

9 I. Meager, R. S. Ashraf, S. Mollinger, B. C. Schroeder, H. Bronstein, D. Beatrup, M. S. Vezie, T. Kirchartz, A. Salleo, J. Nelson, I. McCulloch,, *J. Am. Chem. Soc.* **2013**, *135*, 11537–11540.

10 M. A. Uddin, T. H. Lee, S. Xu, S. Y. Park, T. Kim, S. Song, T. L. Nguyen, S. Ko, S. Hwang, J. Y. Kim, H. Y. Woo, *Chem. Mater.* **2015**, *27*, 5997–6007.

11 W. Li, K. H. Hendriks, A. Furlan, M. M. Wienk, R. A. Janssen, *J. Am. Chem. Soc.* **2015**, *137*, 2231–2234.

12 K. C. Lee, S. Song, J. Lee, D. S. Kim, J. Y. Kim, C. Yang, *ChemPhysChem* **2015**, *16*, 1305–1314.

13 Y. Li, *Acc. Chem. Res.* **2012**, *45*, 723–733.

14 C. Cui, Wai-Yeung Wong, Y. Li, *Energy Environ. Sci.* **2014**, *7*, 2276–2284.

15 C. Cui, Z. He, Y. Wu, X. Cheng, H. Wu, Y. Li, Yong Cao, Wai-Yeung Wong, *Energy Environ. Sci.* **2016**, *9*, 885–891.

16 M. Gao, J. Subbiah, Paul, B. Geraghty, M. Chen, B. Purushothaman, X. Chen, T. Qin, D. Vak, Fiona, H. Scholes, Scott, E. Watkins, M. Skidmore, Gerard, J. Wilson, Andrew, B. Holmes, David, J. Jones, Wallace, W. H. Wong, *Chem. Mater.* **2016**, *28*, 3481–3487.

17 L. Huo, T. Liu, X. Sun, Y. Cai, Alan, J. Heeger, Y. Sun, *Adv. Mater.* **2015**, *27*, 2938–2944.

18 T. I. Ryu, Y. Yoon, J.-H. Kim, D.-H. Hwang, M. J. Ko, D.-K. Lee, J. Y. Kim, H. Kim, N.-G. Park, B. Kim, H. J. Son, *Macromolecules* **2014**, *47*, 6270–6280.

19 H.–J. Yun, Y.–J. Lee, S.–J. Yoo, D. S. Chung, Y.–H. Kim, S. K. Kwon, *Chem. Eur. J.* **2013**, *19*, 13242–13248.

20 J. Kim, A.–R. Han, J. H. Seo, J. H. Oh, C. Yang, *Chem. Mater.* **2012**, *24*, 3464–3472.

21 S. Park, B. T. Lim, B. S. Kim, H. J. Son, D. S. Chung, *Nature* **2014**, *4*, 5482.

22 Yun, H.–J. Kang, S.–J. Yong, X. Kim, S. O. Kim, Y.–H. Noh, Y.–Y. Kwon, S.–K. *Adv. Mater.* **2014**, *26*, 73.00–7307.

23 H.–J. Yun, M. C. Hwang, S. M. Park, R. Kim, D. S. Chung, Y.–H. Kim, S.–K. Kwon, *ACS Appl. Mater. Interfaces* **2013**, *5*, 6045–6053.

24 G. Kim, S. Song, J. Lee, T. Kim, T. H. Lee, B. Walker, J. Y. Kim, C. Yang, *Adv. Energ. Mater.* **2015**, *5*, n/a–n/a.

25 J. Kim, M. H. Yun, G. H. Kim, J. Lee, S. M. Lee, S. J. Ko, Y. Kim, G. K. Dutta, M. Moon, S. Y. Park, D. S. Kim, J. Y. Kim, C. Yang, *ACS Appl. Mater. Interfaces* **2014**, *6*, 7523–7534.